Journal of ELECTRONIC MATERIALS, Vol. 49, No. 2, 2020
https://doi.org/10.1007/s11664-019-07858-4
© 2019 The Minerals, Metals & Materials Society

Spray Deposition of *n*-type Cobalt-Doped CuO Thin Films: Influence of Cobalt Doping on Structural, Morphological, Electrical, and Optical Properties

HASSAN ZARE ASL [1,3] and SEYED MOHAMMAD ROZATI [2]

1.—Department of Physics, Behbahan Khatam Alanbia University of Technology, Behbahan, Iran.
2.—Department of Physics, University of Guilan, Rasht, Iran. 3.—e-mail: Zare@bkatu.ac.ir

The effects of cobalt (Co)-doping (0 at%, 2 at%, 4 at%, 6 at%, and 10 at%) on the structural, morphological, electrical, and optical characteristics of spray-deposited nanostructured copper oxide (CuO) thin films were investigated. X-ray diffraction patterns revealed that the crystallite size is subject to a constant reduction with an increase in the doping concentration. Based on field-emission scanning electron microscopy images, no change was observed for the grain shapes; however, the grain size decreased with an increase in the doping concentration. Furthermore, doping Co led to a conversion from a fairly weak *p*-type conductivity for the undoped CuO thin film (3.42×10^{-4} Ω cm) to a considerable *n*-type conductivity for the 10 at% Co-doped CuO (CuO:Co) film (4.20×10^{-1} Ω cm). Although the mobility of the resulting films decreased with Co doping, it seems that the significant enlargement in free electron carrier concentration is responsible for conductivity transition and improvement. Finally, the bandgap values were estimated using experimental data of transmittance and reflectance.

Key words: Co-doped CuO, thin film, spray pyrolysis, doping concentration, physical properties

INTRODUCTION

Copper oxide (CuO) has been used in many electronic and optoelectronic devices, including thin film solar cells,[1] photoelectrochemical cells,[2] thin film transistors,[3] cross-point memories,[4] and gas sensors,[5] over recent decades. The main advantages of this oxide include the low cost of production, thermal stability, nontoxicity, and relatively high optical absorption.[6]

The fact that CuO thin film can be deposited by almost all conventional methods (namely spin-coating,[7] sputtering,[8] electrodeposition,[9] thermal oxidation,[10] and spray pyrolysis[11]) makes it a suitable option for many researchers. Through numerous studies conducted in recent years, CuO thin films have been prepared using the aforementioned methods. These studies investigated the influence of different parameters such as deposition temperature,[12] the annealing process,[13] nozzle–substrate distance,[14] precursor molarity,[15] solvent properties,[16] and deposition time.[17] Considering that introducing impurities can effectively alter the physical properties of the resulting thin films, researchers have been encouraged to optimize the characteristics of CuO thin films using a proper dopant. Baturay et al.[18] deposited Ni-doped CuO thin films using the spin-coating technique and modified the electrical and optical properties of the films. Masudy-Panah et al.[19] employed Ti to enhance the conductivity of sputter-deposited CuO thin films. This group prepared heterojunction solar cells of a CuO thin film on *n*-type Si and found that the short circuit current and efficiency were significantly improved after introducing Ti into the CuO thin film structure. In the case of the other common

(Received July 13, 2019; accepted November 20, 2019; published online December 2, 2019)

phase of copper oxide (Cu_2O), some researchers have tried to introduce proper dopants to the structure and to achieve *n*-type Cu_2O thin films. Cai et al.[20] used indium as a donor and deposited *n*-type indium-doped Cu_2O thin films by direct current magnetron co-sputtering. Xu et al.[21] deposited pure-phase Cu_2O films via pulsed laser deposition and reported that nitrogen plasma treatment changes dominant point defects from Cu vacancies to O vacancies and results in a transition from a *p*-type to an *n*-type conductivity. To the best knowledge of the authors, however, the influence of cobalt (Co) doping on the physical properties of CuO thin films has hardly been studied. Bayansal et al.[22] employed successive ionic layer adsorption and reaction to grow Co-doped CuO (CuO:Co) thin films and reported considerable changes in their structural, morphological, and optical properties. El Sayed et al.[23] examined the structural, optical, and photocatalytic properties of spin-coated Fe and Co-doped CuO thin films. They found that the Fe and Co-doped CuO thin films, compared with undoped and Fe-doped CuO thin films, exhibit a better photocatalytic degradation of methylene blue. Tawfik et al.[24] deposited pure and Co-doped CuO thin films via DC and AC reactive magnetron sputtering technique, and found that the resistivity decreases with the increase of Co concentration. Furthermore, they investigated the photosensitivity of the resulting films.

In the present study, the spray pyrolysis technique was employed to deposit CuO:Co thin films, and their structural, morphological, electrical, and optical properties were investigated. It is of note that, despite the cost-effectiveness and suitability of this method for mass production, it is a solution-based technique that makes the doping process quite manageable.[25]

Experimental Details

In order to deposit CuO:Co thin films, 0.1-M solutions of copper chloride monohydrate (1.705 g in 100 ml water) and cobalt acetate tetrahydrate (0.249 g in 10 ml water) in double-distilled water were prepared separately. Subsequently, appropriate amounts of the solutions were mixed with [Co]/[Co] + [Cu] proportions of 0 at%, 2 at%, 4 at%, 6 at%, and 10 at%. To deposit each thin film, 20 ml of the resulting solution was spray-deposited into a well-cleaned soda-lime glass substrate using a homemade spray pyrolysis apparatus with a custom glass gun. Afterward, 0.9-bar compressed filtered air was employed to atomize the solution, and the nozzle–substrate distance and substrate temperature were kept at 29 cm and 450°C, respectively.

X-ray diffraction (XRD) patterns of the CuO:Co thin films were recorded using an X'Pert PRO PANalytical diffractometer with Cu-Kα radiation and 0.026 scan steps. A field-emission scanning electron microscope (FESEM; MIRA3TESCAN-XMU) was utilized to study the surface morphology and record the energy-dispersive x-ray spectroscopy (EDX) of the CuO:Co thin films. All the FESEM images were taken with 15.0 kV accelerating voltage and 150 kx magnification. In order to investigate the influence of Co doping on the electrical properties, the mobility, carrier concentration, and resistivity of the prepared films were measured by the Van der Pauw and Hall effect techniques (Phys Tech). Finally, the optical transmittance and reflectance were recorded using a Perkin-Elmer Lambda 25 spectrophotometer.

RESULTS AND DISCUSSION

Structural Properties

Figure 1 shows the XRD patterns of the CuO:Co thin films prepared by the spray pyrolysis technique with different doping concentrations (0, 2, 4, 6, and 10 at%). As can be observed, there are two dominant peaks, at $\sim$ 35.5° and $\sim$ 38.7°, which are the properties of monoclinic CuO (JCPDS Card no. 045-0937). No peaks related to the other common phase of copper oxide (Cu_2O) or to cobalt oxide was observed, indicating the complete substitution of Cu atoms with Co atoms in the CuO structure. To gain a better understanding of the structural properties, the crystallite sizes of the grown CuO:Co thin films were calculated for the two major peaks using the Scherrer equation:

$$D = \frac{0.94\lambda}{\beta \cos\theta} \quad (1)$$

where λ is the wavelength of the x-rays, β is the full width at half-maximum of the diffraction peaks, and θ is the Bragg's diffraction angle.[26,27] Additionally, the lattice constants (i.e., a, b, c, and γ) of the monoclinic CuO along with the thickness values of the resulting films were calculated and are listed in Table I. The results show that increasing the Co

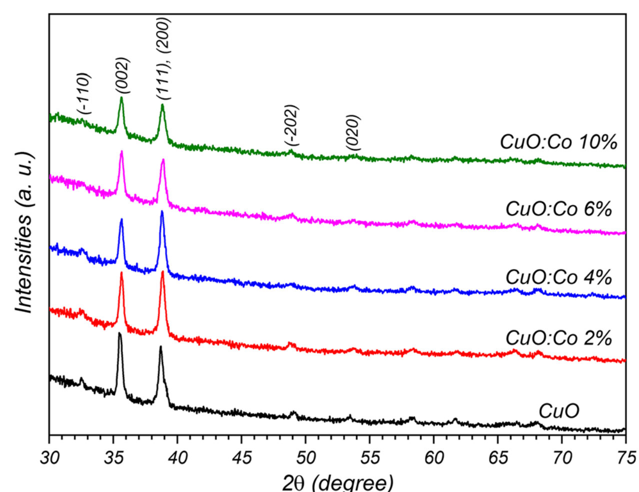

Fig. 1. XRD patterns of CuO:Co thin films with 0, 2, 4, 6, and 10 at% of Co doping.

Table I. Thickness and structural parameters of CuO:Co thin films with 0, 2, 4, 6, and 10 at% of Co doping

Dopant concentration (%)	Peak position 2θ (°)		Thickness t (nm)	Lattice parameters a (Å)	b (Å)	c (Å)	β (°)	V (Å³)	Crystallite size (002) nm	(111), (200) nm
0	35.535	38.728	602	4.679	3.428	5.112	99.068	80.981	24	20
2	35.612	38.814	571	4.677	3.412	5.100	98.968	80.390	22	20
4	35.631	38.832	543	4.677	3.411	5.099	99.054	80.317	22	19
6	35.615	38.828	507	4.678	3.411	5.102	99.110	80.399	21	18
10	35.628	38.840	390	4.677	3.412	5.099	99.022	80.351	18	17

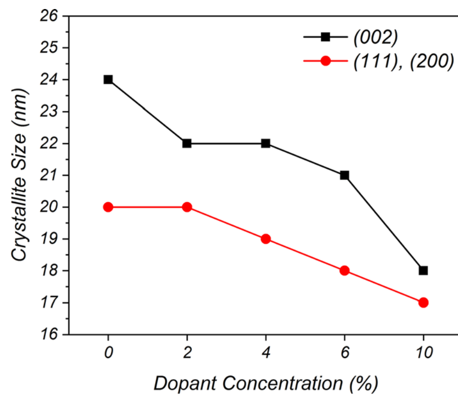

Fig. 2. Calculated crystallite size variation of prominent peaks for the CuO:Co thin films.

concentration in CuO thin films leads to a reduction in the intensity of the dominant peaks (Fig. 1), which might be due to a considerable reduction in the thickness of the films after introducing the Co atoms to the CuO thin film structure.[28] It seems that increasing the incorporation of cobalt acetate tetrahydrate in the precursor causes deviation from the optimum grown condition of the CuO thin films, and thus a thickness reduction. Based on the variation of the calculated size represented in Fig. 2, the calculated crystallite size slightly reduces as the Co concentration increases. This behavior can be attributed to increasing lattice disorder by virtue of increasing Co atoms in the CuO thin film structure. The same effect has been reported for Co doping by Bayansal et al.[22]

Morphological Properties

The systematic variation in the morphology of the spray-deposited CuO:Co thin film with Co concentrations of 0 at%, 2 at%, 4 at%, 6 at%, and 10 at% is shown in Fig. 3. The surface morphology of the films indicates island-like grains with quite distinguishable boundaries, in which the grain size steadily decreases with increasing Co concentration. As can be seen in Fig. 3, the grains for the undoped CuO, compared with the CuO:Co thin films, are more packed with a wider size distribution. Introducing Co to the CuO thin film structure led to the formation of smaller grains (mostly less than 50 nm) with more homogenous size distributions and porous surfaces. However, the reduction of the grain size might partially be related to the thickness reduction of the films with increasing doping concentration. Some studies have investigated the effect of film thickness on the morphology of the resulting CuO thin films and have revealed that thickness reduction can be responsible for the shrinking of grains.[29–31]

To investigate the elemental composition, EDX analysis was performed on the prepared CuO:Co thin films (Fig. 4). The atomic and weight ratios of the detected elements (Table II) confirm the existence of Co atoms in the CuO:Co thin film structures. The presence of Si and Ca and the abundance of O are due to the low thickness of the film and, therefore, the detection of the substrate (soda-lime glass) elements.

Electrical Properties

The electrical properties (i.e., resistivity, mobility, and carrier concentration) of the CuO:Co thin films with different Co doping concentrations prepared by spray pyrolysis technique are summarized in Table III. Furthermore, the variation of the measured resistivity, mobility, and carrier concentration are depicted in Fig. 5. To measure these parameters, the Hall effect technique with the Van der Pauw coplanar contacts was performed on 7×7 mm^2 CuO:Co thin films at room temperature.

As shown in Fig. 5, the mobility of the prepared CuO:Co thin films generally decreased with increasing Co doping percentage, which seems to be correlated with the crystallite and grain size variations. As mentioned in the previous section, the calculated crystallite size decreased with Co doping increase. Reduction in crystallite size can lead to an increase in the number of dangling bonds and therefore barrier height in the crystallite boundaries.[17,32] Furthermore, it is well known that a packed morphology with larger grain size favors better mobility.[33] These effects can adequately explain the mobility variation trend of the resulting CuO:Co thin films.

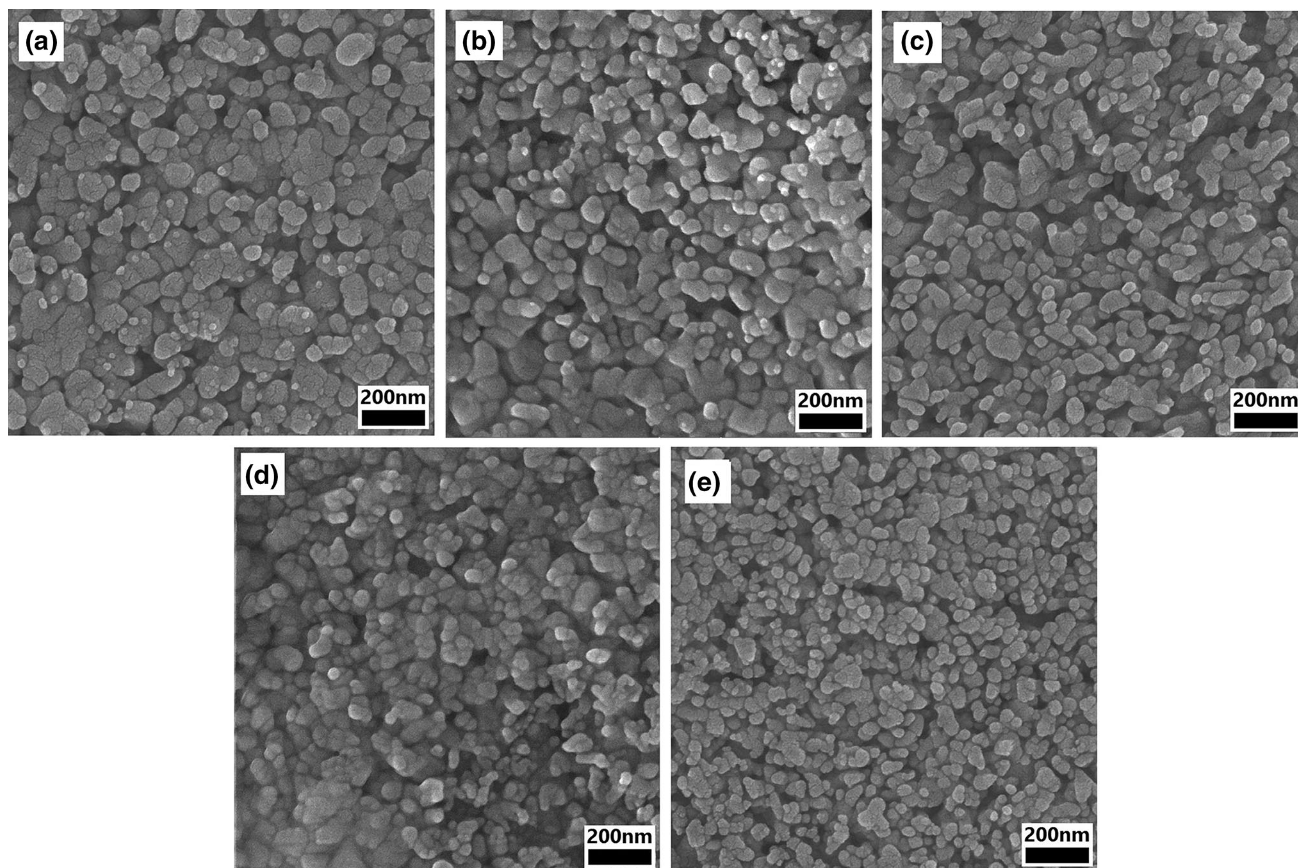

Fig. 3. Surface FESEM images of CuO:Co thin films with (a) 0 at% Co doping, (b) 2 at% Co doping, (c) 4 at% Co doping, (d) 6 at% Co doping, and (e) 10 at% Co doping.

Cu vacancies have been reported as the most stable defects in CuO, and a convincing argument for the intrinsically p-type conductivity of CuO.[34] As shown in Table III, the carrier concentration increases from + 5.00 $\times$ 10^{+14} cm^{-3} for the undoped CuO to $-$ 6.18 $\times$ 10^{+18} cm^{-3} for the 10 at% CuO:Co thin film, which further compensates for the mobility decrease and leads to a considerable reduction in the resistivity of the spray-deposited CuO:Co thin films. There are two common oxidation states for Co: Co^{2+} and Co^{3+} with the ionic radii of 0.745 Å and 0.61 Å, respectively.[35] The significant enlargement in the n-type conductivity of the resulting films indicates the substitution of Cu^{2+} atoms with Co^{3+} in the CuO structure. Moreover, the XRD result confirmed the substitution of Co^{3+} in the CuO structure. Since the ionic radius of Co^{3+} (0.61 Å) is smaller than that of Cu^{2+} (0.73 Å), one can observe a gradual shift in peak positions toward a higher angle for the CuO:Co thin films prepared with Co doping.[36]

Optical Properties

In order to investigate the influence of Co doping on the optical properties, the optical transmittance and reflectance of the prepared CuO thin films were recorded in the range of 200–1000 nm (Fig. 6a). All the resulting thin films showed strong absorption in the visible region (400–600 nm), which gradually decreased in the infrared region. As the Co content increases, the absorption in the visible region (the region of strong absorption) slightly decreases, while the films exhibit more absorption in the near-infrared region (weak absorption region). As discussed earlier, increasing Co doping leads to thickness reduction. Hence, an absorption reduction in the visible region for the CuO thin films can be logically expected. In addition, it is well documented that the absorption in the weak absorption region is the result of defects and impurities,[37] which can adequately explain the absorption rise in the near infra-red region with increasing Co incorporation.

For further clarification, the bandgap (E_g) values of the CuO:Co thin films were estimated using Tauc plots[38–40] (Fig. 6b). To this end, the absorption coefficient (α) was calculated using the experimental transmittance (T) and reflectance (R) data as follows:

$$\alpha = \frac{1}{t}\ln\left[\frac{(1-R^2)}{2T} + \sqrt{\frac{(1-R)^4}{4T^2} + R^2}\right] \quad (2)$$

where t stands for thickness.[41,42]

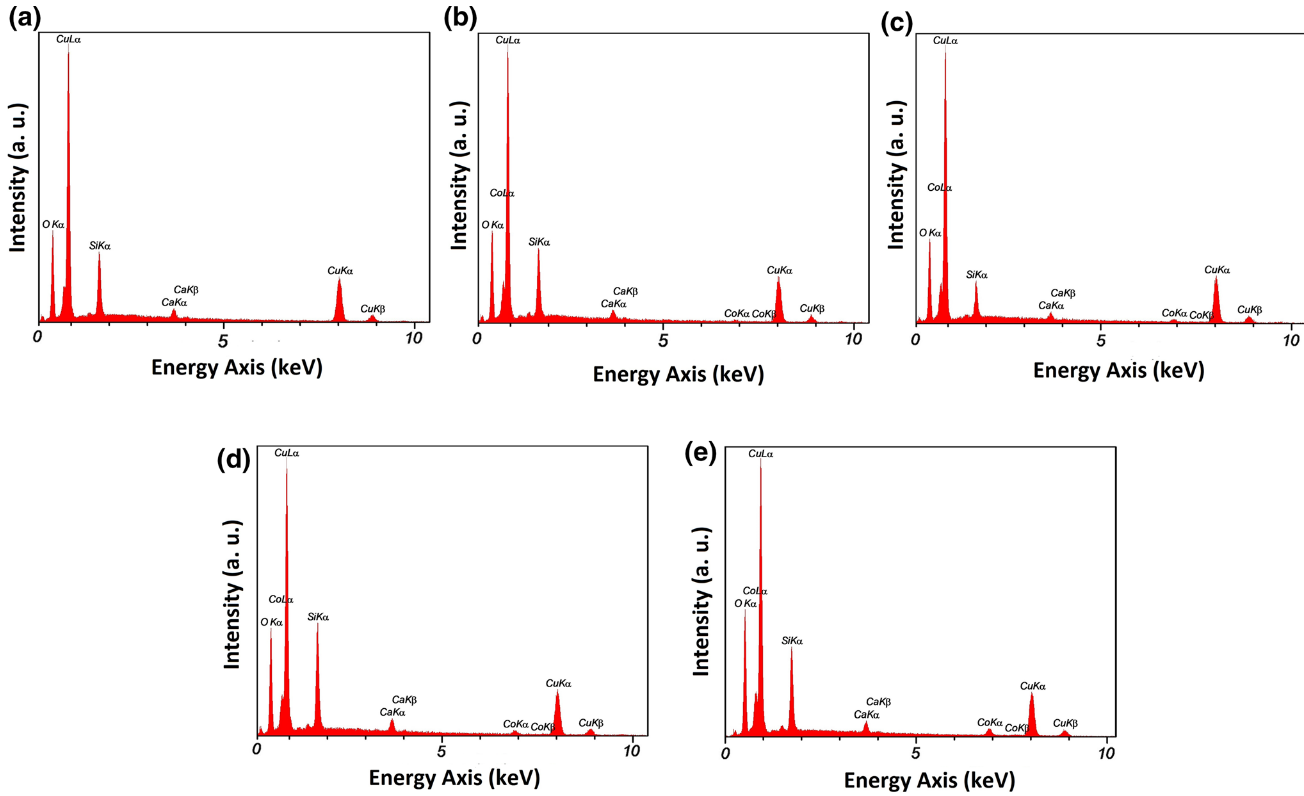

Fig. 4. EDX spectra of CuO:Co thin films with (a) 0 at% Co doping, (b) 2 at% Co doping, (c) 4 at% Co doping, (d) 6 at% Co doping, and (e) 10 at% Co doping.

Table II. Elemental composition of spray-deposited CuO:Co thin films with 0, 2, 4, 6, and 10 at% of Co doping, recorded by EDX analysis

Dopant concentration	O		Cu		Co	
(%)	A%	W%	A%	W%	A%	W%
0	61.57	28.74	38.43	71.26	0	0
2	61.91	29.05	37.81	70.46	0.28	0.49
4	63.19	30.23	36.09	68.57	0.72	1.20
6	64.67	31.59	34.34	66.62	0.99	1.78
10	67.31	34.25	30.58	61.79	2.11	3.96

Table III. Measured electrical properties, estimated bandgap, and Urbach energy of spray-deposited CuO:Co thin films with 0, 2, 4, 6, and 10 at% of Co doping

Dopant concentration (%)	Carrier type	Mobility μ ($cm^2 V^{-1} s^{-1}$)	Carrier concentration (cm^{-3})	Resistivity ρ (Ω cm)	Band gap E_g (eV)	Urbach energy E_U (eV)
0	p	4.28	$+ 5.00 \times 10^{+14}$	2.92×10^3	1.682	0.583
2	n	2.23	$- 3.68 \times 10^{+15}$	7.59×10^2	1.677	0.589
4	n	4.56×10^{-1}	$- 2.87 \times 10^{+17}$	4.77×10^1	1.660	0.608
6	n	2.83×10^{-1}	$- 4.97 \times 10^{+17}$	4.44×10^1	1.652	0.643
10	n	4.26×10^{-1}	$- 6.18 \times 10^{+18}$	2.38×10^0	1.626	0.772

The Urbach energy (E_U), which is especially the case for poor crystalline semiconductors,[37,43] was estimated for the prepared CuO:Co thin films by adopting the following equation:

$$\alpha = \alpha_0 \exp\left(\frac{h\nu}{E_U}\right)a \quad (3)$$

where α_0 is a constant and $h\nu$ is the photon energy. Inverting the slope of Ln(α) versus photon energy ($h\nu$) near the bandgap (Fig. 7a), the Urbach energy can be estimated.[44,45] The estimated values of bandgap and Urbach energy for the spray-deposited CuO:Co thin films are listed in Table III and the variations are shown in Fig. 7b. The results show that the largest estimated bandgap belonged to the undoped CuO thin film (1.682 eV). Introducing Co atoms to the CuO structure led to a constant reduction in the estimated bandgap values from 1.677 eV for 2 at% to 1.626 eV for 10 at%. The resulting bandgap values are in good agreement with the reported values for CuO thin films deposited by spray pyrolysis technique.[12,46] As discussed earlier, increasing the Co content led to increasing disorders and the XRD results confirmed this finding. The presence of disorders in poor crystalline materials results in the formation of localized states that extend into the bandgap (called the Urbach tail) and thus narrow the bandgap in such materials.[47] The correlation between the Urbach energy variation and the derived bandgap for the CuO:Co thin films is quite noticeable. The lowest value of Urbach energy belongs to the undoped CuO (0.583 eV) with the largest band gap

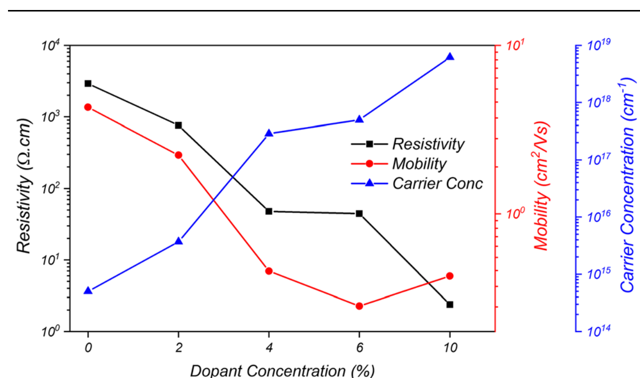

Fig. 5. Variation of resistivity, mobility, and carrier concentration of spray-deposited CuO:Co thin films with 0 at%, 2 at%, 4 at%, 6 at%, and 10 at% of Co doping.

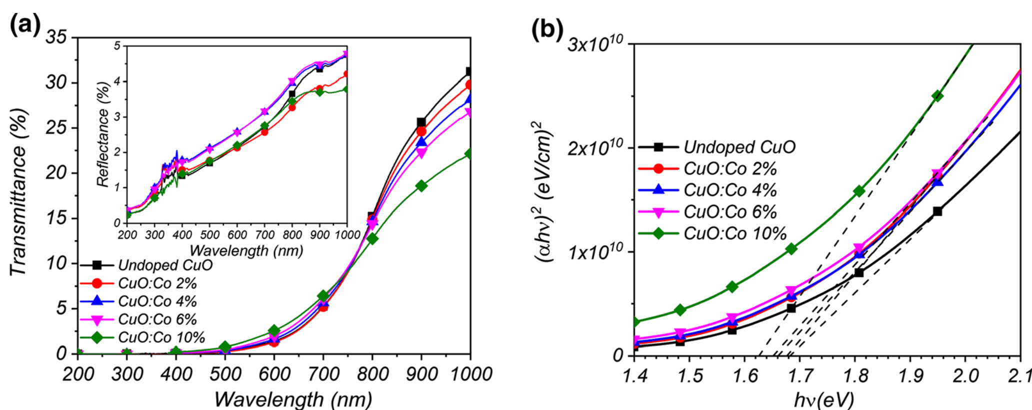

Fig. 6. (a) Optical transmittance of resulting CuO:Co thin films with 0 at%, 2 at%, 4 at%, 6 at%, and 10 at% of Co doping; inset the optical reflectance spectra. (b) Plots of $(\alpha h\nu)^2$ as a function of photon energy to estimate optical bandgap.

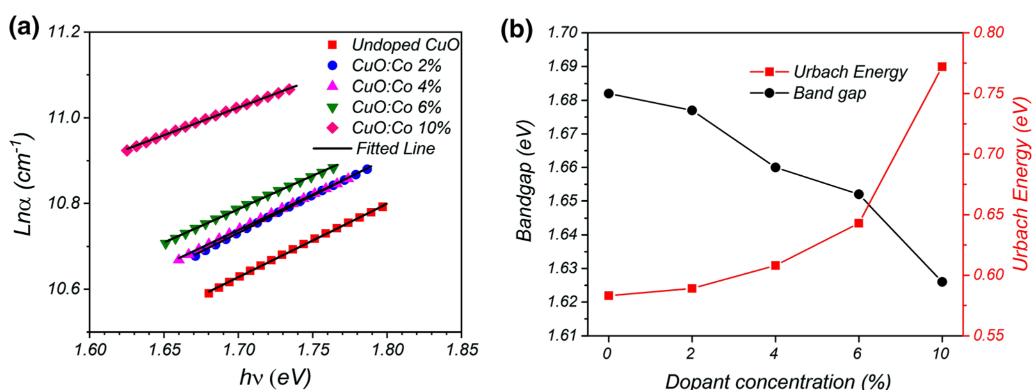

Fig. 7. (a) Plot of Lnα versus hν, (b) the variation of bandgap and Urbach energy for the resulting CuO:Co thin films with 0 at%, 2 at%, 4 at%, 6 at%, and 10 at% of Co doping.

(1.682 eV). The Urbach energy increases with increasing Co doping concentration from 0.589 eV for 2 at% (E_g= 1.677 eV) to 0.772 eV for 10 at% (E_g= 1.626 eV). The same behavior has been reported in the literature for CuO:Co thin films.[22]

CONCLUSION

CuO:Co thin films were successfully deposited into a glass substrate using the spray pyrolysis technique. Then, the effects of Co doping on the structural, morphological, electrical, and optical properties were studied. It was found that, with increasing Co content, the crystallite size decreases, the grain shape remains almost unchanged, the average grain size reduces significantly, and the estimated bandgaps decrease slightly. In addition, introducing Co atoms into the CuO structure led to the conversion from *p*-type to *n*-type conductivity and a considerable reduction in resistivity, which is the direct result of the enlargement in the free electron carrier concentration of the resulting films. Considering that the spray pyrolysis technique is a cost-effective method with high suitability for mass production, the resulting CuO:Co thin films are a wise choice for many semiconductor oxide-based devices.

CONFLICT OF INTEREST

The authors declare that they have no conflict of interest.

REFERENCES

1. A. Bhaumik, A. Haque, P. Karnati, M.F.N. Taufique, R. Patel, and K. Ghosh, *Thin Solid Films* 572, 126 (2014).
2. Y. Chaudhary, *Int. J. Hydrog. Energy* 29, 131 (2004).
3. K.C. Sanal, L.S. Vikas, and M.K. Jayaraj, *Appl. Surf. Sci.* 297, 153 (2014).
4. B.S. Kang, S.-E. Ahn, M.-J. Lee, G. Stefanovich, K.H. Kim, W.X. Xianyu, C.B. Lee, Y. Park, I.G. Baek, and B.H. Park, *Adv. Mater.* 20, 3066 (2008).
5. H. Deng, H.-R. Li, F. Wang, C.-X. Yuan, S. Liu, P. Wang, L.-Z. Xie, Y.-Z. Sun, and F.-Z. Chang, *J. Mater. Sci. Mater. Electron.* 27, 6766 (2016).
6. Q. Zhang, K. Zhang, D. Xu, G. Yang, H. Huang, F. Nie, C. Liu, and S. Yang, *Prog. Mater Sci.* 60, 208 (2014).
7. D.M. Jundale, P.B. Joshi, S. Sen, and V.B. Patil, *J. Mater. Sci. Mater. Electron.* 23, 1492 (2012).
8. C.-C. Hsu, C.-H. Wu, and S.-Y. Wang, *J. Alloys Compd.* 663, 262 (2016).
9. B. Yan, Y. Wang, T. Jiang, and X. Wu, *J. Mater. Sci. Mater. Electron.* 27, 5389 (2016).
10. A.D. Faisal and W.K. Khalef, *J. Mater. Sci. Mater. Electron.* 28, 18903 (2017).
11. J. Morales, L. Sánchez, F. Martín, J.R. Ramos-Barrado, and M. Sánchez, *Thin Solid Films* 474, 133 (2005).
12. V. Saravanan, P. Shankar, G.K. Mani, and J.B.B. Rayappan, *J. Anal. Appl. Pyrolysis* 111, 272 (2015).
13. F.A. Akgul, G. Akgul, N. Yildirim, H.E. Unalan, and R. Turan, *Mater. Chem. Phys.* 147, 987 (2014).
14. R.J. Deokate, A.V. Moholkar, G.L. Agawane, S.M. Pawar, J.H. Kim, and K.Y. Rajpure, *Appl. Surf. Sci.* 256, 3522 (2010).
15. R. Shabu, A. Moses Ezhil Raj, C. Sanjeeviraja, and C. Ravidhas, *Mater Res. Bull.* 68, 1 (2015).
16. H.Z. Asl and S.M. Rozati, *J. Electron. Mater.* 46, 5020 (2017).
17. I. Singh and R.K. Bedi, *Appl. Surf. Sci.* 257, 7592 (2011).
18. S. Baturay, A. Tombak, D. Kaya, Y.S. Ocak, M. Tokus, M. Aydemir, and T. Kilicoglu, *J. Sol-Gel. Sci. Technol.* 78, 422 (2016).
19. S. Masudy-Panah, K. Radhakrishnan, H.R. Tan, R. Yi, T.I. Wong, and G.K. Dalapati, *Sol. Energy Mater. Sol. Cells* 140, 266 (2015).
20. X.-M. Cai, X.-Q. Su, F. Ye, H. Wang, X.-Q. Tian, D.-P. Zhang, P. Fan, J.-T. Luo, Z.-H. Zheng, G.-X. Liang, and V.A.L. Roy, *Appl. Phys. Lett.* 107, 083901 (2015).
21. M. Xu, X. Liu, W. Xu, H. Xu, X. Hao, and X. Feng, *J. Alloys Compd.* 769, 484 (2018).
22. F. Bayansal, T. Taşköprü, B. Şahin, and H.A. Çetinkara, *Metall. Mater. Trans. A* 45, 3670 (2014).
23. A.M. El Sayed and M. Shaban, *Spectrochim Acta Part A* 149, 638 (2015).
24. W.Z. Tawfik, Z.S. Khalifa, M.S. Abdel-wahab, and A.H. Hammad, *J. Mater. Sci. Mater. Electron.* 30, 1275 (2018).
25. M. Eslamian, *Coatings* 4, 60 (2014).
26. B.D. Cullity, *Elements of X-ray Diffraction*, 1st ed. (Boston: Addision-Wesley, 1956), pp. 96–102.
27. W.Z. Tawfik, A.A. Farghali, A. Moneim, N.G. Imam, and S.I. El-Dek, *Nanotechnology* 29, 215709 (2018).
28. C. Abdelmounaïm, Z. Amara, A. Maha, and D. Mustapha, *Mater. Sci. Semicond. Process.* 43, 214 (2016).
29. Y. Akaltun, *Thin Solid Films* 594, 30 (2015).
30. V. Dhanasekaran, T. Mahalingam, and V. Ganesan, *Microsc. Res. Tech.* 76, 58 (2013).
31. J. Morales, L. Sánchez, F. Martín, J.R. Ramos-Barrado, and M. Sánchez, *Electrochim. Acta* 49, 4589 (2004).
32. Y. Kajikawa, *J. Appl. Phys.* 114, 053707 (2013).
33. D. Gopalakrishna, K. Vijayalakshmi, and C. Ravidhas, *Ceram. Int.* 39, 7685 (2013).
34. D. Wu, Q. Zhang, and M. Tao, *Phys. Rev. B* 73, 235206 (2006).
35. R. Shannon, *Acta Crystallogr. Sect. A Found. Crystallogr.* 32, 751 (1976).
36. H. Behzad, F.E. Ghodsi, and H. Karaağaç, *Ionics* 23, 2429 (2017).
37. A.S. Hassanien and A.A. Akl, *Superlattices Microstruct.* 89, 153 (2016).
38. J. Tauc, R. Grigorovici, and A. Vancu, *Phys. Status Solidi B* 15, 627 (1966).
39. H.Z. Asl and S.M. Rozati, *J. Mater. Sci. Mater. Electron.* 29, 4365 (2018).
40. M.M.A. Ahmed, W.Z. Tawfik, M.A.K. Elfayoumi, M. Abdel-Hafiez, and S.I. El-Dek, *J. Alloys Compd.* 791, 586 (2019).
41. H.Z. Asl and S.M. Rozati, *J. Electron. Mater.* 47, 3568 (2018).
42. H. Behzad and F.E. Ghodsi, *J. Mater. Sci. Mater. Electron.* 27, 6096 (2016).
43. J. Melsheimer and D. Ziegler, *Thin Solid Films* 129, 35 (1985).
44. L. Chabane, N. Zebbar, M. Kechouane, M.S. Aida, and M. Trari, *Thin Solid Films* 605, 57 (2016).
45. K.A. Aly, A.M. Abd Elnaeim, M.A.M. Uosif, and O. Abdel-Rahim, *Physica B* 406, 4227 (2011).
46. M. Lamri Zeggar, L. Chabane, M.S. Aida, N. Attaf, and N. Zebbar, *Mater. Sci. Semicond. Process.* 30, 645 (2015).
47. A.S. Hassanien and A.A. Akl, *J. Alloys Compd.* 648, 280 (2015).

Publisher's Note Springer Nature remains neutral with regard to jurisdictional claims in published maps and institutional affiliations.